Erbium in oxygen-doped silicon: Electroluminescence

S. Lombardo and S. U. Campisano
Dipartimento di Fisica della Università, Corso Italia, 57, I-95129 Catania, Italy

G. N. van den Hoven and A. Polman
FOM Institute for Atomic and Molecular Physics, Kruislaan 407, 1098 SJ Amsterdam, The Netherlands

(Received 15 November 1994; accepted for publication 30 January 1995)

Room-temperature electroluminescence at 1.54 μm is demonstrated in erbium-implanted oxygen-doped silicon (27 at. % O), due to intra-4f transitions of the Er^{3+}. The luminescence is electrically stimulated by biasing metal-(Si:O, Er)-p^+ silicon diodes. The 30-nm-thick Si:O, Er films are amorphous layers deposited onto silicon substrates by chemical-vapor deposition of SiH_4 and N_2O, doped by ion implantation with Er to a concentration up to $\approx$1.5 at. %, and annealed in a rapid thermal annealing furnace. The most intense electroluminescence is obtained in samples annealed at 400 °C in reverse bias under breakdown conditions and it is attributed to impact excitation of erbium by hot carriers injected from the Si into the Si:O, Er layer. The electrical characteristics of the diode are studied in detail and related to the electroluminescence characteristics. A lower limit for the impact excitation cross section of $\approx 6\times10^{-16}$ cm^2 is obtained. © *1995 American Institute of Physics.*

I. INTRODUCTION

Many approaches to obtain efficient light emission from silicon are under intense investigation because of many potential applications. As the feasibility of other elementary devices such as detectors,[1,2] waveguides,[3] and modulators has already been demonstrated, the realization of an efficient silicon light source is crucial for the application of Si technology to optoelectronics and optical telecommunication. In addition, the growing complexity and speed of silicon integrated circuits will require the use of optical interconnects and thus the integration of devices for optical communication.

Unfortunately, due to its indirect band gap, silicon is characterized by a low probability for radiative electron-hole recombination;[4] for this reason silicon light-emitting diodes show a very poor near-infrared band-edge luminescence. Therefore, many alternative approaches are currently investigated. One possibility is to reduce the concentration of defects that promote nonradiative recombination. Indeed, in silicon devices with highly passivated surfaces, characterized by very long carrier lifetimes, somewhat enhanced quantum efficiencies for radiative recombination have been reported.[5] Another approach is based on the use of epitaxial Ge_xSi_{1-x} alloys or Si-Ge superlattices, which may show a nearly direct band gap.[6] The recent development of Ge_xSi_{1-x} deposition techniques[7,8] and the knowledge of the process limits for avoiding misfit dislocation formation and layer intermixing, have permitted the fabrication of devices using defect-free materials. In these, near-infrared electroluminescence attributed to band-to-band recombination has been demonstrated at low temperatures.[9] Unfortunately, a strong luminescence quenching occurs at increasing temperature, and the quantum efficiency becomes low at room temperature. A very promising development is that of porous silicon,[10,11] for which intense room-temperature photoluminescence has been demonstrated already in the near-infrared–to–visible range. Large quantum efficiencies are observed both in hydrogen passivated and in thermal oxidized materials[12] but problems related to mechanical fragility, low thermal conductivity, as well as the attainment of efficient electroluminescence still remain unsolved.

An alternative way is the doping of silicon by erbium. The Er^{3+} ion is characterized by complete external 5s and 5p shells and an incomplete internal 4f shell. The external shells shield the 4f electrons from the influence of the host material and sharp atomiclike intra-4f transitions are observed.[13] The transition involving the ground state $^4I_{15/2}$ and the first excited state $^4I_{13/2}$ corresponds to a wavelength of $\approx$1.54 μm, which coincides with the window of maximum transmission in silica-based optical fibers. Therefore, many researchers have investigated the possibility of electrically exciting this transition in silicon. The first demonstration of erbium-related electroluminescence in a silicon light-emitting diode (LED) was reported by Ennen *et al.*[14] who showed the occurrence of luminescence at 1.54 μm in a forward-biased LED fabricated by molecular-beam epitaxy of Si doped during deposition by Er ion implantation. Unfortunately, strong luminescence quenching was observed with increasing temperature,[15,16] and this effect rendered the luminescence not measurable at room temperature.

Subsequently it was pointed out that oxygen and other impurities enhance the Er^{3+} luminescence.[15,17] Oxygen forms complexes with erbium[18] producing two positive effects: first, an increase in luminescence intensity, and second, a marked decrease of the luminescence quenching with temperature.[19,20] By codoping silicon with Er and O, room-temperature electroluminescence at 1.54 μm has been achieved recently in light-emitting diodes, both in forward and in reverse bias above the breakdown voltage.[21,22]

The fundamental role played by oxygen in Er doping of silicon led us to investigate the Er doping of heavily oxygen-doped silicon thin films deposited by chemical-vapor deposition of SiH_4 and N_2O. The material is a solid mixture of silicon and silicon oxide phases usually indicated as semi-insulating polycrystalline silicon (SIPOS). The acronym

 0021-8979/95/77(12)/6504/7/$6.00 © 1995 American Institute of Physics

Downloaded 15 Sep 2003 to 131.215.237.184. Redistribution subject to AIP license or copyright, see http://ojps.aip.org/japo/japcr.jsp

SIPOS will be used throughout this work and indicates the material described above even though our work is focused more on amorphous rather than polycrystalline materials. SIPOS is a high-resistivity semiconductor, normally used in silicon technology, particularly for the passivation of edge structures in power devices.[23,24] The carrier transport mechanisms in this material have been studied and are related to its microstructure.[25,26] The large oxygen concentrations, lying in the 1–60 at. % range, and its compatibility with Si technology render this semiconductor a very attractive host for Er.

In a previous article,[27] SIPOS films containing 4, 10, and 27 at. % O were implanted with Er ions and annealed at a temperature in the 300–1100 °C range in order to recover the ion implantation damage and optically activate the erbium. Intense room-temperature Er-related photoluminescence at 1.54 μm was observed in all the samples: The maximum signal was revealed in the material containing 27 at. % O and annealed at 500 °C. In addition, excitation spectroscopy measurements showed that the Er excitation is produced via the recombination of electron-hole pairs which transfer their recombination energy to the Er.

These results led us to investigate the Er luminescence under electrical excitation performed by biasing suitable metal-SIPOS-silicon structures: In this article we report the results of this study demonstrating for the first time in this material room-temperature electroluminescence and a very weak luminescence quenching with temperature. The mechanisms leading to the electroluminescence are discussed and the cross section for Er excitation is experimentally evaluated. A detailed experimental study of Er in SIPOS under optical excitation will be reported elsewhere.[28]

II. EXPERIMENT

Silicon wafers of 125 mm diameter, (100) oriented, polished on both sides, B-doped (10–20 Ω cm) were implanted with 80 keV B at fluences of 5×10^{13} and 2×10^{15} cm^{-2} on front and back sides, respectively. For dopant activation, the samples were processed in a rapid thermal annealing (RTA) apparatus at 1000 °C for 5 min in a N_2 ambient. After removal of the native oxide by dipping in a diluted HF solution, SIPOS was deposited by chemical-vapor deposition of SiH_4 and N_2O at 620 °C. The process resulted in 30-nm-thick layers containing 27 at. % O. Oxygen content and thickness of the layers were measured by Rutherford backscattering spectrometry (RBS) of 2 MeV ^{4}He at a scattering angle of 102°. Cross-sectional transmission electron microscopy on the front side of the samples confirmed that the SIPOS thickness was 30 nm and showed that the underlying silicon after B implantation and diffusion was damage free. The samples were then implanted with 35 keV Er at an angle of 60° from the surface normal in order to confine all the erbium inside the SIPOS layer; the doses were 2.5 or 5×10^{14} cm^{-2}. At the highest fluence the sputtered thickness was $\approx$1.5 nm and the Er peak concentration was $\approx$1.6 at. %, located at a depth of $\approx$9 nm, as evaluated by numerical simulations of the implantation process and confirmed by RBS.

After annealing in a RTA for 5 min in a N_2 ambient at a temperature between 400 and 1000 °C, Ti-Ni-Au metal contacts were deposited through a mask in an ultrahigh-vacuum e-beam evaporator, defining a Burrus-type geometry with a circular contact of 0.16 cm^2 on the front and a complementary metallization on the back side. A schematic drawing of the resulting structure is shown in Fig. 1. Due to the high resistivity of the SIPOS layer the current is confined in the cylindric volume under the contact on SIPOS and is then spread in the low-resistivity silicon substrate. The infrared light produced by biasing the device is collected from the back side; at 1.5 μm wavelength the Si absorption coefficient[29] is less than 1 cm^{-1} and thus the infrared light is essentially unattenuated by traversing the 600-μm-thick silicon substrate. The external collection efficiency, limited mainly by total internal reflection, amounts to $\approx$2% for a 2π sr collection efficiency.[30]

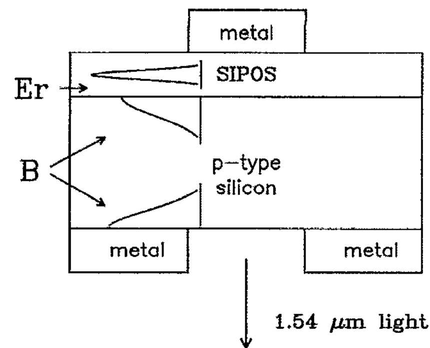

FIG. 1. Schematic cross section of the metal-SIPOS-p^+ silicon diode structure used for the electroluminescence measurements.

Electroluminescence (EL) was studied by biasing the diodes between −35 and +15 V with the samples held at a temperature in the 200–400 K range. Diode polarization is assumed to be forward when the potential of the p-type silicon substrate is positive with respect to the metal contact on the SIPOS layer. The light was collected by a lens system, focused in a single grating spectrometer with 6 nm resolution and then detected by a Ge detector cooled at liquid-nitrogen temperature. The device was biased by a square-wave current signal at 40 Hz produced by a power amplifier driven by a function generator; to improve the signal-to-noise ratio a lock-in amplification technique was used. EL decay measurements were performed by switching off the current and recording the luminescence signal on a digital oscilloscope; the overall response time of the system was less than 30 μs.

III. RESULTS AND DISCUSSION

A. Electroluminescence

Figure 2 shows the electroluminescence signal observed at room temperature at −20 V bias with a current of 260 mA in a sample implanted with 5×10^{14} Er/cm^2 and annealed at 400 °C. The spectrum shown is similar to those observed in photoluminescence[27,28] and can be attributed to $^4I_{13/2}\rightarrow{}^4I_{15/2}$ transitions in Er^{3+}.

It is the sample implanted with 5×10^{14} cm^{-2} and annealed at 400 °C in which the largest electroluminescence is observed and the data shown below refer to this device. Elec-

Downloaded 15 Sep 2003 to 131.215.237.184. Redistribution subject to AIP license or copyright, see http://ojps.aip.org/japo/japcr.jsp

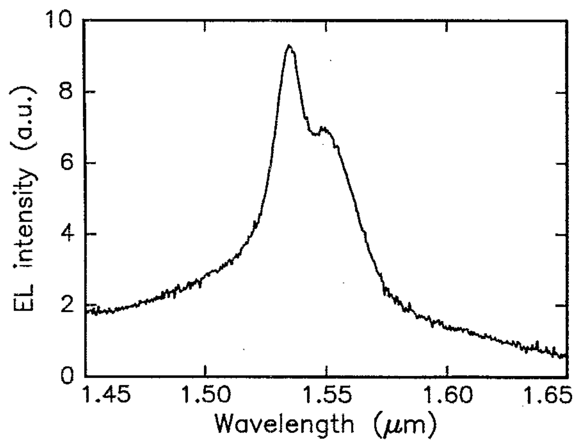

FIG. 2. Electroluminescence spectrum taken at room temperature in reverse bias in a device in which SIPOS was implanted with an Er dose of 5×10^{14} cm^{-2} and annealed at 400 °C. The SIPOS metal contact was positively biased with respect to the p^+ silicon to a voltage of 20 V and the resulting current was 260 mA.

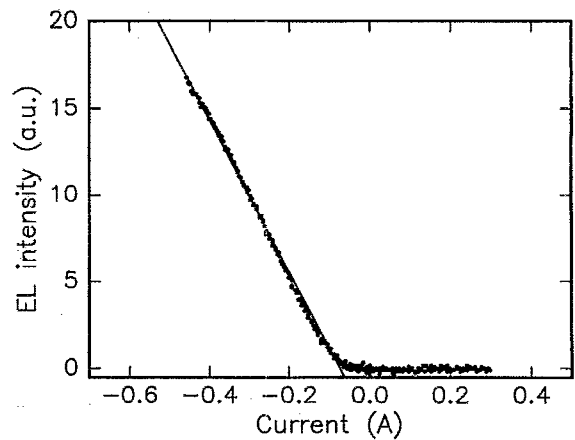

FIG. 4. Electroluminescence intensity at 1.54 μm measured at room temperature as a function of the current in the device of which the I-V characteristics are shown in Fig. 3. The solid line is a fit used to extrapolate the threshold current.

troluminescence was also observed in samples implanted at 2.5×10^{14} Er/cm^2 and/or annealed at temperatures above 400 °C, but in this case the intensities were lower. The trend of electroluminescence intensity as a function of anneal temperature is very similar to that of the photoluminescence, and will be discussed in detail in Ref. 28. Note that the Er-implanted SIPOS annealed at 400 °C has an amorphous structure.

It is important to underline that clear luminescence is observed only in reverse bias when the device is fully in breakdown. In forward bias a small signal is observed in devices annealed at 500 and 600 °C (not shown), but the intensity measured at the largest current level (≈400 mA) is approximately a factor of 10 smaller than the signal shown in Fig. 2.

Figure 3 shows the I-V characteristics of the device at room temperature. The main features of the characteristics are a large differential resistance between ≈−3 and 0 V and nearly linear I-V characteristics at large positive and negative biases, characterized by differential resistances of ≈25 and 30 Ω, respectively.

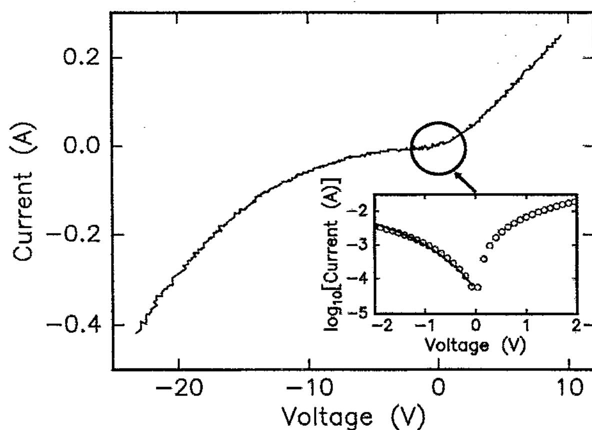

FIG. 3. I-V characteristics measured at 300 K of the device in which SIPOS has been implanted with 5×10^{14} Er/cm^2 and annealed at 400 °C. The inset shows the I-V characteristics (solid circles) in a lower-bias region together with a theoretical curve (solid line) calculated according to Eq. (1).

Figure 4 shows the electroluminescence intensity at 1.54 μm as a function of the current flowing in the device; it is apparent that in reverse bias the EL intensity increases linearly with current above a threshold of 75 mA, while it is at the noise level in forward bias. The almost perfect signal linearity in reverse bias occurs also when it is plotted as a function of the voltage because the intense luminescence is observed in the linear region of the I-V characteristics; the threshold voltage is −14.5 V.

By increasing the temperature from 200 to 400 K, the threshold current, voltage, and slope of the EL signal versus current (not shown) shift slightly toward lower values, resulting in a very small quenching effect of the electroluminescence for increasing temperature. Such a small quenching effect is also observed in photoluminescence.[28]

B. Electrical characteristics

The observed electroluminescence can be understood by knowing the carrier transport mechanisms in the device. Consequently, we will divide the discussion of the data into a first part describing the electrical conduction models, and a second part discussing the electroluminescence.

The hole concentration profile in the silicon under the SIPOS was measured by the spreading resistance technique: The profile, reported in Fig. 5, shows a carrier concentration equal to 1×10^{15} cm^{-3} at the SIPOS-silicon interface; the concentration increases with depth reaching a maximum at ≈250 nm of nearly 2×10^{18} cm^{-3} and then decreases reaching the substrate concentration value at a depth of ≈700 nm. The boron chemical profile obtained by the SUPREM IV code[31] is also shown in Fig. 5: In the 0–130 nm surface region the boron concentration is much higher than the carrier concentration, and it ranges from 5×10^{16} cm^{-3} at the surface up to 5×10^{17} cm^{-3} at ≈130 nm. By comparing boron and hole

Downloaded 15 Sep 2003 to 131.215.237.184. Redistribution subject to AIP license or copyright, see http://ojps.aip.org/japo/japcr.jsp

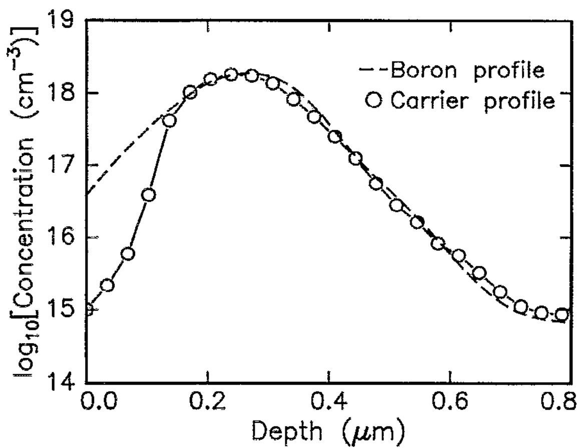

FIG. 5. Hole concentration profile measured by spreading resistance in the silicon under the SIPOS implanted with 80 keV B at 5×10^{13} cm^{-2}. Also shown is the boron chemical profile obtained by SUPREM IV simulation.

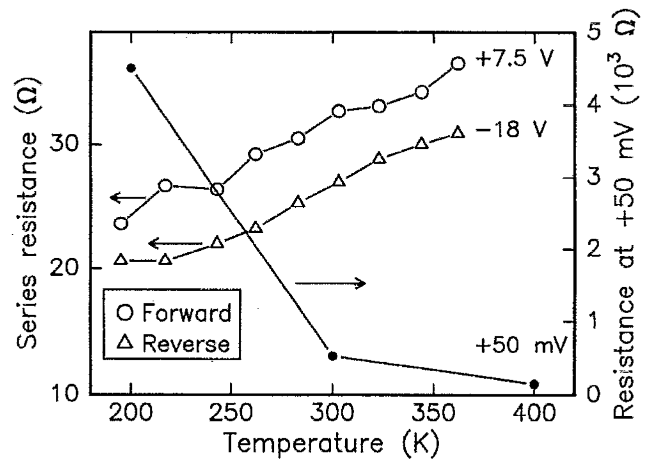

FIG. 7. Differential resistances of the device of which the characteristics are reported in Fig. 3 as a function of temperature. Open circles and triangles and solid circles refer to the voltage ranges $+7.5\pm2.5$ and -17.5 ± 2.5 V and $+50\pm10$ mV, respectively.

profiles we conclude that the 130-nm-thick surface layer is depleted of mobile carriers; moreover, since the carrier concentration at the surface is about 1×10^{15} cm^{-3}, we conclude that the Fermi level is pinned at the Si-SIPOS interface at a value about 0.29 eV above the valence-band edge. Using Gauss's theorem, the electric field at the SIPOS-p^+ silicon junction in thermal equilibrium is estimated to be approximately 2.5×10^5 V/cm in silicon, and $\approx5\times10^5$ V/cm in SIPOS, assuming a ratio of about two between the dielectric constants of SIPOS and silicon.[32]

On the basis of these considerations the simplified band diagram at thermal equilibrium of the metal-SIPOS-p^+ Si structure is as shown in Fig. 6(a). The SIPOS film has an amorphous microstructure and at low electric fields shows hopping conductivity.[33] As sketched in Fig. 6(a), we expect that SIPOS will show a mobility gap larger than the crystalline Si forbidden gap. This is also confirmed by the fact that the fundamental absorption edge of SIPOS occurs at a higher proton energy than that observed in amorphous silicon.[32]

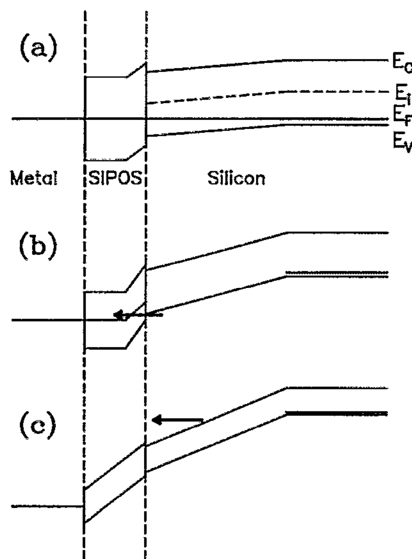

FIG. 6. Band diagrams of the metal-SIPOS-p^+ silicon diode in thermal equilibrium (a) and in reverse bias at low (b) and high (c) voltages. The arrow in (b) shows the tunneling path of electrons which produces the leakage current of the diode at low reverse biases. The arrow in (c) indicates hot electrons injected from the Si depletion layer into the SIPOS. Note that the relative scales of (a), (b), and (c) are not the same.

On the basis of the band diagram of Fig. 6(a), we can model the I-V characteristics of the device. For this purpose, the temperature dependences of the differential resistances at +7.5 and −17.5 V and +50 mV were measured, and they are shown in Fig. 7. In the case of large biases the resistances increase with temperature; note that the resistance measured in forward bias is always larger than that measured in reverse bias. Vice versa, the device resistance measured at low forward bias shows a marked decrease by increasing temperature. The striking differences in the behavior of the differential resistances at low and high voltages can be attributed to different conduction regimes.

In forward bias most of the voltage is applied across the SIPOS film because the metal-SIPOS and the SIPOS-p^+ Si junctions introduce negligible resistances, and thus the electrical characteristics are entirely due to the SIPOS layer. At low forward bias carrier transport will occur by hopping as confirmed by the temperature dependence of the differential resistance at +50 mV and by the high corresponding resistivity values (10^8 Ω cm at 300 K). At large forward biases the strength of the electric field in SIPOS is large and the transport is due to tunneling of carriers moving through localized states up to several tenths of an eV above the Fermi level, since large tunnel probabilities are expected. The occurrence of tunneling is confirmed by the low value and the weak temperature dependence of the resistance. The small increase of the differential resistance with temperature can be attributed to the decrease of carrier mobility and lifetime.

In reverse bias the situation is different: At low voltages the bias is almost entirely applied to the SIPOS-p^+ Si junction and not to the SIPOS layer, as sketched in Fig. 6(b); the current in this case is limited by the tunneling of valence-

Downloaded 15 Sep 2003 to 131.215.237.184. Redistribution subject to AIP license or copyright, see http://ojps.aip.org/japo/japcr.jsp

band electrons of silicon toward free localized states in SIPOS of energies above the Fermi level [arrow in Fig. 6(b)]. Consequently the current is proportional to the tunnel probability f_T throughout the barrier of height $E_F - E_V \approx 0.29$ eV, as indicated by the spreading resistance measurements. f_T is given by[30]

$$f_T = \exp\left(-\frac{8\pi(2m^*)^{1/2}(E_F - E_V)^{3/2}}{3qhE_{el}} \right), \quad (1)$$

where m^* is the electron effective mass, q the electron charge, and h is the Planck constant. The electric field in SIPOS at the junction E_{el} can be assumed to be equal to $\approx 4V/W_{Si} + E_{el}^{in}$,[30] where V is the reverse applied voltage, W_{Si} is the silicon depletion layer thickness evaluated by the spreading resistance measurement, and E_{el}^{in} is the thermal equilibrium field in SIPOS at the junction ($\approx 5 \times 10^5$ V/cm). E_{el} is evaluated by assuming that the silicon depletion layer field depends linearly on the depth and assuming that the ratio between the dielectric constants of silicon and SIPOS is 2. As the reverse bias current is proportional to f_T, we can fit the low reverse bias characteristics; the inset of Fig. 3 shows the experimental I-V characteristics at low voltages (circles) together with the best-fit curve obtained assuming $E_F - E_V = 0.29$ eV. The good agreement confirms that in low reverse bias the current is limited by tunneling at the junction from Si to SIPOS.

At large reverse biases the tunnel probability f_T approaches unity, and the voltage will be shared between the SIPOS film and the SIPOS-p^+ silicon junction, as shown in Fig. 6(c). The electric field at the SIPOS-p^+ silicon junction in the silicon side is then approximately equal to $V/(2W_{SIPOS} + 1/2W_{Si})$,[30] where W_{SIPOS} is the SIPOS layer thickness; thus, at -14 V bias the field in the Si will reach a value of $\approx 1 \times 10^6$ V/cm which will cause a breakdown by the occurrence of a combination of avalanche and Zener mechanisms.[30] The breakdown produces in the p^+ silicon conduction band a large density of hot electrons directed toward the SIPOS layer.

At this point it is possible to explain why the differential resistance measured at large reverse biases is smaller than that measured in forward bias, as shown in Fig. 7. In this large reverse bias regime, the SIPOS layer will conduct by tunneling as in the case of large forward bias; but there will also be an additional current contribution due to the hot electrons coming from the p^+ silicon region. We can estimate the relative contributions of tunneling and hot carriers to the total current on the basis of the measured values of resistance. By subtracting the substrate series resistance (5 Ω) and taking into account the voltage sharing between the SIPOS layer and the SIPOS-p^+ silicon junction, we find that at -18 V reverse bias both tunnel and hot carrier current are approximately of the same order of magnitude. This implies that under breakdown conditions, in the SIPOS layer 50% of the total current consists of hot electrons.

C. Impact excitation

The EL measurements (Fig. 4) show that in reverse bias the electroluminescence at 1.54 μm is much more efficient than that observed in forward polarization. The EL signal increases linearly with current only in reverse bias above a threshold, while it is almost zero in forward bias: The same trend is observed at any temperature in the 200–400 K range. Note that the threshold bias at which the EL signal starts to increase is about 14 V, which corresponds approximately with the breakdown in the silicon depletion layer. Moreover, since at these biases the I-V characteristics are almost linear, a further increase of the voltage produces a linear increase of the current and of the EL signal.

These characteristics suggest that the mechanism by which the Er^{3+} is excited is impact excitation by hot electrons coming from the silicon depletion layer. In fact, when the breakdown is reached, the carrier temperature is extremely high and can be estimated by solving the Boltzmann transport equation. In the presence of large fields, the carriers acquire an energy of the order of $qE_{el}\lambda$, where E_{el} is the electric field in the silicon depletion layer and λ is the mean free path for optical phonon collisions (≈ 6 nm).[30] The scattering probability is isotropic and thus the average increase of carrier kinetic energy can be estimated to be approximately $(qE_{el}\lambda)^2/4E_p$, where E_p is the energy lost by optical-phonon collision;[34] using this simple approach, the average carrier energy is of the order of ≈ 2 eV in our case. A more detailed approach also takes into account energy loss by impact creation of electron-hole pairs. This interaction is characterized by a larger energy loss than the optical-phonon collisions, and by a much larger mean free path (≈ 50 nm).[30] Taking both mechanisms into account, the carrier distribution in velocity space is nearly spherically symmetric and Maxwellian. The temperature of the Maxwell distribution is extremely high and field dependent; in our case, at the threshold bias it results about 0.65 eV.[34] Then, according to our former estimate, above the threshold roughly half of the total current flowing in the SIPOS layer is given by hot electrons whose temperature is 0.65 eV. This implies that a significant fraction of them will have enough energy to excite the Er^{3+} ions (at least ≈ 0.8 eV).

In forward polarity, on the other hand, this mechanism is not active because the field in the silicon depletion layer is insufficient to produce a large electron temperature since the bias decreases the field with respect to its value at thermal equilibrium; the small forward bias electroluminescence observed in the devices annealed at 500 and 600 °C (not shown) may be attributed to an electron-hole recombination process in which the recombination energy is transferred to the Er^{3+} ion, and it is characterized by a small quantum efficiency.

The occurrence of an impact excitation mechanism for the electroluminescence in reverse bias is supported by the weak temperature dependence of the phenomenon. As temperature is increased we only observe a small decrease of the threshold bias and current, which tentatively can be explained by the decrease of the silicon band gap. This decrease, in fact, produces the decrease of the breakdown voltage for the Zener mechanism occurring in the silicon depletion layer. With increasing temperature, we also observe a weak decrease of the slope of the EL signal versus

Downloaded 15 Sep 2003 to 131.215.237.184. Redistribution subject to AIP license or copyright, see http://ojps.aip.org/japo/japcr.jsp

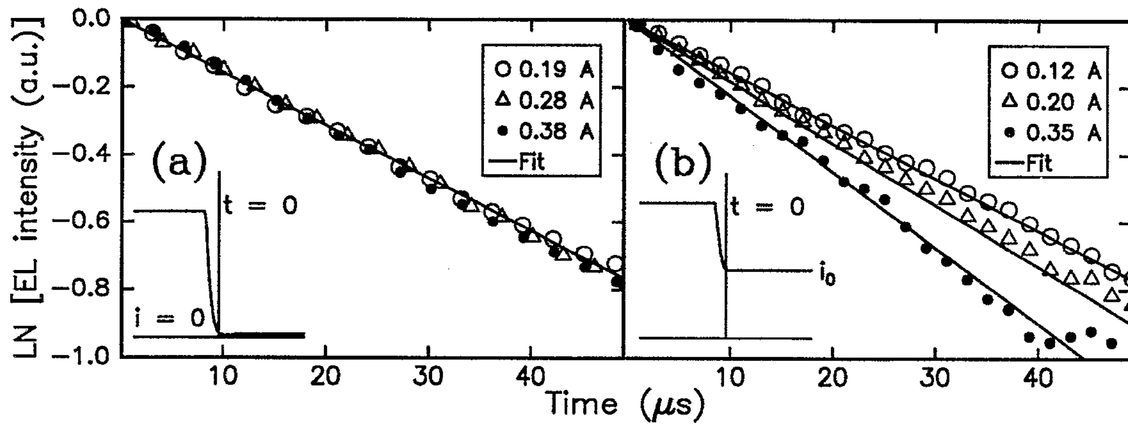

FIG. 8. Normalized EL decay transients. (a) Decay for three different initial steady-state currents (indicated in the figure) after that current is switched off. (b) Decay from a initial steady-state current as the current is suddenly reduced to a lower (non-zero) level (i_0, indicated in the figure). Only the transient decay is shown, i.e., the final steady-state level is subtracted from the data.

current, which can be attributed to the increase of the series resistance with temperature.

D. Impact excitation cross section

In order to determine the cross section for impact excitation of Er^{3+} we have measured the transients of EL intensity at 1.54 μm by switching the current source. The normalized time evolution of the luminescence after switching off is reported in Fig. 8(a): The time constant appears unaffected by the initial current level and is $\approx$70 μs. An interesting behavior is observed when the current is rapidly switched from a high level to a lower value. In this case, the EL signal rapidly decays to a new (lower) steady-state level. The transient of the EL to this second level is plotted in Fig. 8(b). It shows an exponential trend but the time constant depends on the second current level (i_0): The time constant decreases with increasing currents.

Figure 9 shows the EL decay rate (inverse of the time constant) versus the second current level determined from data as in Fig. 8(b). The decay rate increases with the current and the increase is almost linear. These results can be interpreted by a simple two-level model: The Er^{3+} ions are divided into a group N_2 excited to the $^4I_{13/2}$ manifold and in a group N_1 in the ground state ($^4I_{15/2}$). The time derivative of N_2 is given by

$$\frac{dN_2}{dt} = -SN_2 + P(N_0 - N_2), \tag{2}$$

where N_0 is the total number of the Er^{3+} ions, S is the spontaneous emission rate ($N_2 \rightarrow N_1$), and P the pump rate ($N_1 \rightarrow N_2$). When the current is zero, P is zero, because there is no excitation process. In this case, according to Eq. (2), by switching off the device, the transient EL signal will show an exponential decrease with time, with a rate equal to S independent on the initial current level, as confirmed by the data reported in Fig. 8(a). On the other hand, when the current level is switched to a lower value i_0 [Fig. 8(b)], P is nonzero and the transient will be characterized by a rate equal to $(P+S)$. Plotting the decay rate R as a function of i_0 we observe a linear increase, as reported in Fig. 9. This fact implies that P is proportional to the hot carrier flux Φ, and we assume that

$$P \approx \sigma \Phi, \tag{3}$$

where σ is the impact excitation cross section. Φ is the flux of high-energy electrons able to excite the Er and, as discussed before, is comparable to the total flux of carriers. Thus, by fitting the data of Fig. 9 assuming $R \approx \sigma \Phi' + S$ with Φ' equal to the total current density divided by q, we obtain an impact excitation cross section equal to 6×10^{-16} cm^{-2}, which is a reasonable value.[35] This represents a lower limit to the real cross section for two reasons:

(a) according to our former estimate, the flux of hot electrons is about 50% of the total flux;
(b) only a fraction of the hot electrons is able to excite the Er ions because the hot carrier temperature (0.65 eV) is lower than the minimum energy for Er excitation (0.8 eV).

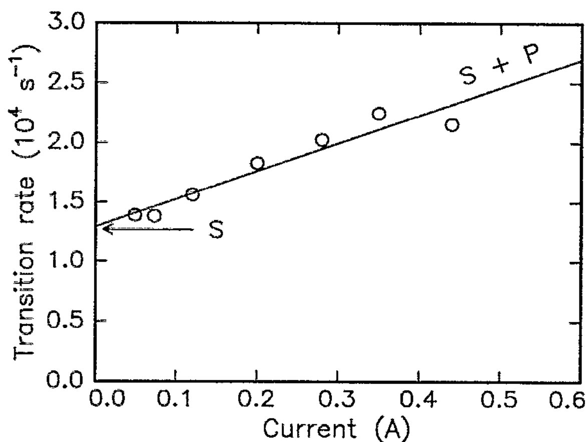

FIG. 9. Decay rate of the EL signal upon switching the current to a lower value as a function of this second current level (i_0). The intercept at $i=0$ corresponds to the spontaneous emission rate S. The drawn line is a fit of $S+P$, with P the pump rate, proportional to the current.

Downloaded 15 Sep 2003 to 131.215.237.184. Redistribution subject to AIP license or copyright, see http://ojps.aip.org/japo/japcr.jsp

Finally, we would like to underline a last important point: From Eq. (2) it follows that the steady-state condition is $N_2/N_1 = P/S$; the data of Fig. 9 indicate that at a current level above ≈0.5 A the ratio N_2/N_1 should overcome 1, or, in other words, it should be possible to obtain population inversion, the first requirement for laser action.

These results are the first experimental evidence of the possibility to fabricate an electrically pumped laser operating at room temperature at a wavelength of 1.54 μm in a silicon-based semiconductor.

IV. CONCLUSIONS

We have demonstrated Er-related electroluminescence at room temperature at 1.54 μm in metal-SIPOS-p^+ silicon structures reverse biased above breakdown. We attribute the electroluminescence to impact excitation of the Er^{3+} ions by hot electrons injected into the Er-doped SIPOS film from the p^+ silicon depletion layer. The carrier temperature is ≈0.65 eV and therefore high enough to produce a large population of electrons able to excite the erbium by impact. The quenching effect of the luminescence with temperature is very weak, and this confirms the validity of the proposed excitation mechanism which is nonthermal. The measurements of the electroluminescence transients under step variations of the pump current have permitted the evaluation of a lower limit for the excitation cross section equal to 6×10^{-16} cm^2, in agreement with what is expected for an impact excitation mechanism.

This work shows that population inversion, which is a fundamental requirement for laser fabrication, can be obtained by electrical excitation in an Er-doped silicon-based semiconductor.

ACKNOWLEDGMENTS

We gratefully acknowledge Dr. V. Privitera for spreading resistance measurements, Professor E. Rimini, Dr. C. Papuzza, and Dr. A. Antonucci for useful discussions, and Professor F. W. Saris for critical reading of the manuscript. We are sincerely indebted to S. Pannitteri, O. Parasole, and A. Marino for technical assistance. Work partially supported by GNSM-CNR. Work at FOM is part of the research program of FOM, and is financially supported by NWO, IOP Electro-optics, and STW.

[1] E. Ahlstrom and W. W. Gartner, J. Appl. Phys. **33**, 2602 (1962).
[2] B. Y. Tsaur, C. K. Chen, and J. P. Mattia, IEEE Electron Device Lett. **EDL-11**, 162 (1990).
[3] R. Olshansky, Rev. Mod. Phys. **51**, 341 (1979).
[4] J. R. Haynes and W. C. Westphal, Phys. Rev. **101**, 1676 (1956).
[5] E. Yablonovitch and T. Gmitter, Appl. Phys. Lett. **49**, 587 (1986).
[6] R. Zachai, K. Eberl, G. Abstreiter, E. Kasper, and H. Kibbel, Phys. Rev. Lett. **64**, 1055 (1990).
[7] B. S. Meyerson, R. J. Uram, and F. K. Legoues, Appl. Phys. Lett. **53**, 2555 (1988).
[8] J. C. Bean, T. T. Sheng, L. C. Feldman, A. T. Fiory, and R. T. Lynch, Appl. Phys. Lett. **44**, 102 (1984).
[9] J. C. Sturm, H. Manoham, L. C. Lenchyshyn, M. L. W. Thewatt, N. L. Rowell, J. P. Noel, and D. C. Houghton, Phys. Rev. Lett. **66**, 1362 (1991).
[10] L. T. Canham, Appl. Phys. Lett. **57**, 1046 (1990).
[11] A. G. Cullis and L. T. Canham, Nature **353**, 335 (1991).
[12] V. Petrova-Koch, T. Muschik, A. Kux, B. K. Meyer, F. Koch, and V. Lehman, Appl. Phys. Lett. **61**, 943 (1992).
[13] S. Hüfner, *Optical Spectra of Transparent Rare Earth Compounds* (Academic, New York, 1978).
[14] H. Ennen, G. Pomrenke, A. Axman, K. Eisele, W. Haydl, and J. Schneider, Appl. Phys. Lett. **46**, 381 (1985).
[15] J. Michel, J. L. Benton, R. F. Ferrante, D. C. Jacobson, D. J. Eaglesham, E. A. Fitzgerald, Y. H. Xie, J. M. Poate, and L. C. Kimerling, J. Appl. Phys. **70**, 2672 (1991).
[16] A. Polman, J. S. Custer, E. Snoeks, and G. N. van den Hoven, Nucl. Instrum. Methods B **80/81**, 653 (1993).
[17] P. N. Favennec, H. L'Haridon, D. Moutonnet, M. Salvi, and M. Gauneau, Jpn. J. Appl. Phys. **29**, 524 (1990).
[18] D. L. Adler, D. C. Jacobson, D. J. Eaglesham, M. A. Marcus, J. L. Benton, J. M. Poate, and P. H. Citrin, Appl. Phys. Lett. **61**, 2181 (1992).
[19] S. Coffa, F. Priolo, G. Franzò, V. Bellani, A. Carnera, and C. Spinella, Phys. Rev. B **48**, 11 782 (1993).
[20] R. Serna, E. Snoeks, G. N. van den Hoven, and A. Polman, J. Appl. Phys. **75**, 2644 (1994).
[21] F. Y. Ren, J. Michel, Q. Sun-Paduano, B. Zheng, H. Kitagawa, D. C. Jacobson, J. M. Poate, and L. C. Kimerling, Mater. Res. Soc. Symp. Proc. **301**, 87 (1993).
[22] G. Franzò, F. Priolo, S. Coffa, A. Polman, and A. Carnera, Appl. Phys. Lett. **64**, 2235 (1994).
[23] T. Matsushita, T. Aoki, T. Otsu, H. Yamoto, H. Ayashi, M. Okayama, and Y. Kawana, Jpn. J. Appl. Phys. Suppl. **15**, 35 (1976).
[24] T. Yamaguchi, K. L. Seaward, J. L. Sachitano, Jr., D. Ritchie, and S. Seto, IEEE J. Solid State Circuits **SC-13**, 472 (1978).
[25] M. L. Tarng, J. Appl. Phys. **49**, 4069 (1978).
[26] S. Lombardo, S. U. Campisano, and F. Baroetto, Phys. Rev. B **47**, 13 561 (1993).
[27] S. Lombardo, S. U. Campisano, G. N. van den Hoven, A. Cacciato, and A. Polman, Appl. Phys. Lett. **63**, 1942 (1993).
[28] G. N. van den Hoven, A. Polman, S. Lombardo, and S. U. Campisano (unpublished).
[29] G. E. Stillman, V. M. Robbins, and N. Tabatabaie, IEEE Trans. Electron Devices **ED-31**, 1643 (1984).
[30] S. M. Sze, *Physics of Semiconductor Devices* (Wiley, New York, 1981).
[31] J. D. Plummer and R. W. Dutton, SRC Technical Report No. T86085, Stanford University, 1986.
[32] G. Compagnini, S. Lombardo, R. Reitano, and S. U. Campisano (unpublished).
[33] N. F. Mott and E. A. Davis, *Electronic Processes in Non-Crystalline Materials* (Oxford University Press, Oxford, 1980).
[34] G. A. Baraff, Phys. Rev. A **135**, 528 (1964), and references therein.
[35] L. C. Feldman and J. W. Mayer, *Fundamentals of Surface and Thin Film Analysis* (North-Holland, New York, 1986), p. 131.

Downloaded 15 Sep 2003 to 131.215.237.184. Redistribution subject to AIP license or copyright, see http://ojps.aip.org/japo/japcr.jsp